Aeroelastic Tailoring of a Strut-Braced Wing for a Medium Range Aircraft

Carrillo Córcoles, X.; De Breuker, R.; Sodja, J.

DOI
10.2514/6.2024-2590

Publication date
2024

Document Version
Final published version

Published in
Proceedings of the AIAA SCITECH 2024 Forum

AIAA SciTech Forum
8-12 January 2024, Orlando, FL
AIAA SCITECH 2024 Forum

10.2514/6.2024-2590

Aeroelastic Tailoring of a Strut-Braced Wing for a Medium Range Aircraft

Xavier Carrillo Córcoles*, Roeland De Breuker † and Jurij Sodja‡

This study explores the implementation of aeroelastic tailoring in the design of a regional aircraft featuring a strut-braced wing (SBW). Making use of the aeroelastic optimisation framework from Delft University of Technology, PROTEUS, the research addresses two distinct cases. The first case involves a simplified SBW geometry to validate the modifications of PROTEUS, which were conducted to include the strut in the aeroelastic analysis. Static and dynamic load cases are compared with a NX Nastran aeroelastic model, showing good agreement in displacements, strains, and gust response. In the second case, the study investigates the weight-saving potential of aeroelastic tailoring in an SBW aircraft based on the ATR-72. Three optimisation scenarios, allowing various laminate types, are examined: unbalanced symmetric laminates, balanced symmetric laminates, and a thickness optimisation with a prescribed balanced symmetric stacking sequence. The results reveal that the prescribed stacking sequence limits stiffness tailoring, thereby also reducing potential weight savings. Moreover, the study shows how the presence of a strut reduces wing deflections, limiting the effectiveness of aeroelastic tailoring.

Nomenclature

Variables

$\hat{D}_{11}$	=	thickness-normalized bending modulus of elasticity, -
E_{11}	=	modulus of elasticity in fiber direction (1), N/m^2
E_{22}	=	modulus of elasticity orthogonal to fiber direction (2), N/m^2
$\hat{E}_{11}$	=	thickness-normalized engineering modulus of elasticity, -
F	=	force, N
G_{12}	=	shear modulus in 1-2 plane, N/m^2
h_c	=	cruise altitude, m
K	=	stiffness matrix, N/m or N/rad
M_c	=	cruise Mach number, -
M_i	=	moment around i$^{\text{th}}$ axis, N$\cdot$ m
N_i	=	i$^{\text{th}}$ node, -
v_c	=	cruise true airspeed, m/s
θ	=	angle with respect to fiber direction (positive clockwise), $[0, 360]$ deg
ν_{12}	=	Poisson's ratio in 1-2 plane, -

List of abbreviations

EAS	=	Equivalent Airspeed
DOF	=	Degree of Freedom
GCMMA	=	Globally Convergent Method of Moving Asymptotes

*Researcher, Faculty of Aerospace Engineering, Aerospace Structures and Computational Mechanics, Kluyverweg 1 2629 HS Delft, X.CarrilloCorcoles@tudelft.nl

†Associate Professor, Faculty of Aerospace Engineering, Aerospace Structures and Computational Mechanics, Kluyverweg 1 2629 HS Delft, R.deBreuker@tudelft.nl, AIAA Associate Fellow

‡Assistant Professor, Faculty of Aerospace Engineering, Aerospace Structures and Computational Mechanics, Kluyverweg 1 2629 HS Delft, J.Sodja@tudelft.nl, AIAA Senior Member

FEM	=	Finite Element Model
HERWINGT	=	Hybrid Electric Regional Wing Integration Novel Green Technologies
LC	=	Load Case
SBW	=	Strut-Braced Wing
SUGAR	=	Subsonic Ultra Green Aircraft Research
TAS	=	True Airspeed
TRL	=	Technology Readiness Level
VLM	=	Vortex Lattice Method

I. Introduction

In 2000, the European Commission set up the Advisory Council for Aviation Research and innovation in Europe to provide guidelines for Europe's aviation sector, serving as the foundation for moving the industry towards greener standards, increased industrial competitiveness and social benefits [1, 2]. With these objectives in mind, the European Union initiated the Clean Sky Joint Undertaking and its subsequent programmes, Clean Sky 2 and Clean Aviation, which were tasked with the implementation of green and innovative technology development. The defined goals of these programmes were clearly outlined in the Flightpath 2050 report from the European Commission [3], which proposed the ambitious steps required to reduce the adverse environmental impact of commercial air travel. With this report, the European Commission set the target of achieving a 75% reduction in CO_2 emissions per passenger per kilometre, a 90% reduction in NO_x and a 65% reduction in perceived noise by 2050, in comparison to aircraft available in the year 2000.

These objectives appear exceptionally challenging for conventional aircraft design as it is becoming increasingly difficult to extract more performance out of the well-known wing and tube configuration. Consequently, unconventional designs are being explored. One promising candidate to overcome these challenges is the Strut-Braced Wing (SBW), in which the strut provides a bending moment relief on the main wing, enabling an increase in the aspect ratio of the wing without the significant weight penalty of a conventional cantilevered wing. This, in turn, reduces induced drag [4], enhancing the aerodynamic efficiency of the aircraft and aiding in emissions reduction.

The SBW configuration has undergone extensive investigation by Virginia Tech Multidisciplinary Aircraft Design Group [5–9], whose work is also part of the Subsonic Ultra Green Aircraft Research (SUGAR) project led by The Boeing Company and studies an SBW concept as part of NASA N+3 concept studies [10]. The project is currently in Phase IV, focusing on increasing the cruise speed to Mach 0.8 and studying the high-lift system performance [11]. These studies have demonstrated the potential of the configuration, with an expected 8% reduction of fuel consumption compared to a cantilever baseline concept. Similarly, ONERA explored the concept in the ALBATROS research project [12], DLR investigated it in the FrEACs project [13], and European-funded projects, such as U-HARWARD [14] and RHEA [15], conducted various multidisciplinary analysis and concluded that the SBW can significantly reduce the operational empty weight with respect to conventional wing-tube aircraft. Furthermore, the AGILE project [16–18] included more detailed structural design studies, introducing aeroelastic tailoring to further reduce the structural weight.

Now, the Hybrid Electric Regional Wing Integration Novel Green Technologies (HERWINGT)[19, 20] project in Clean Aviation is considering the SBW design to address the challenging objectives the industry is facing. The project aims to develop the key technologies to address a new design for a hybrid-electric regional aircraft and make these technologies mature up to technology readiness level 5 (TRL5). Therefore, using the ATR-72 aircraft as a reference and building on the previous work conducted in Clean Sky I and II, the HERWINGT project "aims to design a novel wing, ideal for the future Hybrid-Electric Aircraft of the Regional Segment, and to develop architectures, structures, and technologies allowing higher integration of electric systems" [20].

As part of the HERWINGT project, this study investigates the impact of aeroelastic tailoring on the structural mass of the SBW, which is accomplished by using PROTEUS, the in-house aeroelastic optimisation framework developed at Delft University of Technology [21]. Since the response of the SBW depends on both the main wing and the strut, PROTEUS is modified such that the structural properties of both lifting surfaces are optimised concurrently. Furthermore, PROTEUS allows the modification of the aeroelastic response making use of the stiffness tailoring capabilities of composites. Therefore, exploiting this capability,

this paper explores the advantages of aeroelastic tailoring while fulfilling design constraints such as maximum strains, laminate feasibility, flutter and buckling constraints.

To conclude, this paper is structured as follows. Section II presents the methodology used, including a description of PROTEUS and the necessary modifications to study the SBW. Next, Section III discusses the study cases, featuring a validation case and the optimisation of the HERWINGT wing design. Finally, Section IV analyses the results of these studies and Section V presents the conclusions and next steps.

II. Methodology

The model used for this study is built in PROTEUS, the aeroelastic optimisation framework developed at the Delft University of Technology. This section outlines the PROTEUS framework and the necessary modifications for assessing the SBW.

A. PROTEUS

Figure 1 presents the block diagram of the PROTEUS framework [21]. The optimisation procedure begins with the provision of wing properties and load cases. First, the wing is defined by the aerodynamic shape (airfoils and planform), the structural layout (position of spars and ribs) and the material properties. Additionally, it is possible to define other non-structural mass elements, such as engines or fuel tanks, and control surfaces, both of which influence the load cases.

In order to assess these load cases, PROTEUS supports both linear and nonlinear static aeroelastic analysis and dynamic aeroelastic analysis linearised around the nonlinear static solution. Furthermore, for each load case, it is possible to define the flight conditions and the fuel loads, which have an impact on the mass distribution on the wing.

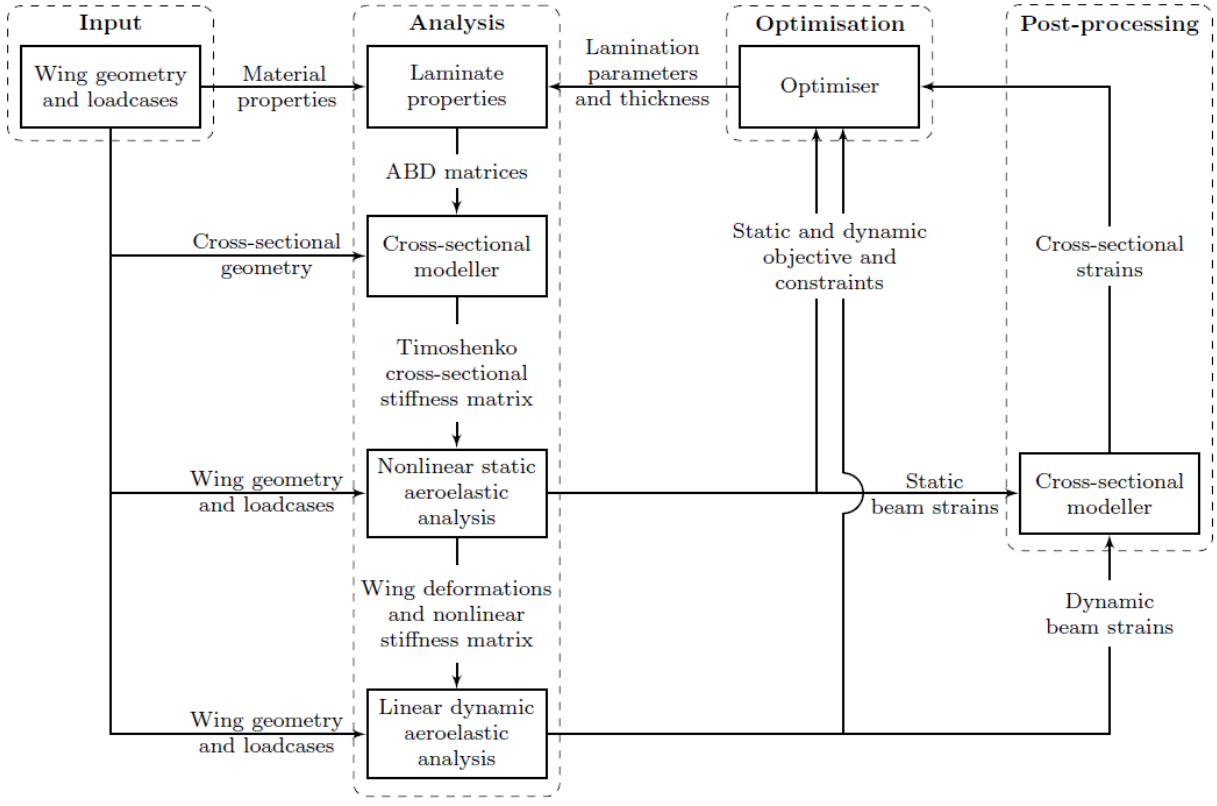

Fig. 1 Block diagram of the PROTEUS framework [21].

Subsequently, these inputs are used to discretise the wing. For the structure, the 3D wing geometry is first reduced to the wingbox and discretised with laminate regions on each of the elements comprising the wingbox (e.g. wing skin, spar webs,...), corresponding to the design regions to be optimised. In each of these regions, a distinct laminate is defined using eight lamination parameters [22] and the laminate thickness. As a result, each region has its own stiffness properties.

Afterwards, the cross-sectional modeller is employed to generate the Timoshenko stiffness matrices, using the laminate properties and wing geometry [23]. This process creates a geometrically nonlinear Timoshenko beam model in co-rotational framework, which can be coupled to the aerodynamic model.

The aerodynamic model employed in this study is based on the Vortex Lattice Method (VLM), which is implemented by discretising the wing into chordwise and spanwise vortex ring elements following the camber line of the wing, as presented by Katz and Plotkin [24]. The aerodynamic forces are calculated for each panel and subsequently transferred to the beam as statically equivalent nodal forces. Furthermore, the model incorporates a Prandtl-Glauert correction factor to account for compressibility, expanding the applicability of the model to high-subsonic flight conditions (Mach < 0.6).

The obtained aeroelastic model is then used to assess the input load cases to obtain the loads and displacements on the structure. The cross-sectional modeller is used to recover the strains in the laminates, which are subsequently used to evaluate the strength and buckling properties of the structure. In addition, the respective sensitivities are computed analytically, allowing for the use of a gradient-based optimiser, the Globally Convergent Method of Moving Asymptotes (GCMMA) developed by Svanberg [25], to evaluate the objective function and constraints.

Finally, the primary objective of the optimisation is the minimisation of the structural weight. Simultaneously, the procedure includes aeroelastic constraints (such as flutter, divergence, control effectiveness), buckling constraints, maximum strain constraints and manufacturing constraints (minimum/maximum thickness, laminate feasibility).

B. SBW implementation

The implementation of the SBW necessitates certain adjustments within the PROTEUS framework. On the structural aspect, the strut is treated as a second wing hence the generation of the wingbox (stiffness and mass matrices) does not require any modifications. Nevertheless, the matrices of both the wing and the strut need to be assembled into a global system, where the wing-strut connection is represented by the shared degrees of freedom (DOFs), which can be visualised in the example presented in Figure 2. In this illustrative example, the wing has m nodes and the strut has n nodes, denoted as N_i^W and N_i^S respectively, with a single DOF per node, u_i^W and u_i^S respectively. This discretisation leads to the wing and strut individual stiffness matrices, $\mathbf{K_W}$ and $\mathbf{K_S}$, as shown in Equation 1. As nodes N_j^W and N_n^S share their DOF, hence $u_j^W = u_n^S$, the resulting global static system of equations is the one presented in Equation 2, where the contributions from $\mathbf{K_W}$ and $\mathbf{K_S}$ are highlighted in blue and red respectively and $\mathbf{F_{ext}}$ is the array of external forces.

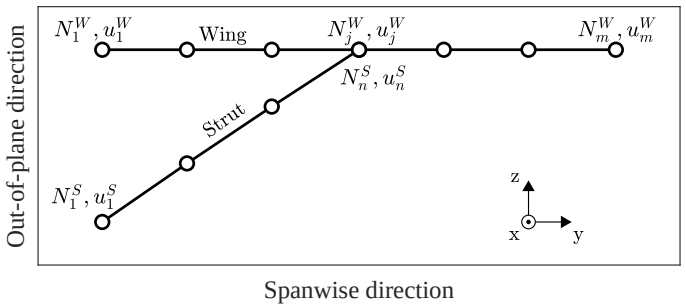

Fig. 2 Example of SBW with a single DOF per node.

$$\mathbf{K_W} = \begin{pmatrix} k^W_{11} & k^W_{12} & 0 & \dots & 0 & 0 \\ k^W_{12} & k^W_{22} & k^W_{23} & \dots & 0 & 0 \\ 0 & k^W_{23} & k^W_{33} & \dots & 0 & 0 \\ \vdots & \vdots & \vdots & \ddots & \vdots & \vdots \\ 0 & 0 & 0 & \dots & k^W_{m-1,m-1} & k^W_{m-1,m} \\ 0 & 0 & 0 & \dots & k^W_{m-1,m} & k^W_{m,m} \end{pmatrix}; \mathbf{K_S} = \begin{pmatrix} k^S_{11} & k^S_{12} & 0 & \dots & 0 & 0 \\ k^S_{12} & k^S_{22} & k^S_{23} & \dots & 0 & 0 \\ 0 & k^S_{23} & k^S_{33} & \dots & 0 & 0 \\ \vdots & \vdots & \vdots & \ddots & \vdots & \vdots \\ 0 & 0 & 0 & \dots & k^S_{n-1,n-1} & k^S_{n-1,n} \\ 0 & 0 & 0 & \dots & k^S_{n-1,n} & k^S_{n,n} \end{pmatrix} \tag{1}$$

$$\mathbf{K_g} \cdot \mathbf{U} = \mathbf{F_{ext}} \rightarrow \begin{pmatrix} k^W_{11} & & & & & \\ & \ddots & & & & \\ & & k^W_{j,j}+k^S_{n,n} & & & k^S_{n-1,n} \\ & & & \ddots & & \\ & & & & k^W_{m,m} & \\ & & k^S_{n-1,n} & & & k^S_{11} \\ & & & & & \ddots \\ & & & & & k^S_{n-1,n-1} \end{pmatrix} \cdot \begin{Bmatrix} u^W_1 \\ \vdots \\ u^W_j \\ \vdots \\ u^W_m \\ u^S_1 \\ \vdots \\ u^S_{n-1} \end{Bmatrix} = \mathbf{F_{ext}} \tag{2}$$

On the other hand, it is not possible to separate the computation of the aerodynamic loads on each component, the wing and the strut, due to the aerodynamic influence between each other. As a result, the loads on both surfaces are computed concurrently using the VLM and subsequently transferred to the corresponding nodes. This process results in the external loads presented in Equation 3 and Equation 4, which are later assembled into the global external forces array, $\mathbf{F_{ext}}$, as presented in Equation 5.

$$\mathbf{F_w} = \left\{ f^W_1, \dots, f^W_m \right\}^T \tag{3}$$

$$\mathbf{F_s} = \left\{ f^S_1, \dots, f^S_n \right\}^T \tag{4}$$

$$\mathbf{F_{ext}} = \left\{ f^W_1, \dots, f^W_j + f^S_n, \dots, f^W_m, f^S_1, \dots, f^S_{n-1} \right\}^T \tag{5}$$

III. Study Cases

This work presents two different study cases. On the one hand, a simplified wing geometry is employed to validate the aeroelastic model by comparing the results to a NX Nastran model. On the other hand, the impact of aeroelastic tailoring on the SBW is explored using the wing geometry of a regional aircraft designed within the HERWINGT project.

A. Case 1: Validation

The primary objective of this study case is to validate the implementation of the SBW in the aeroelastic model. This is accomplished by comparing results obtained from PROTEUS with those obtained using an aeroelastic model implemented in NX Nastran, focusing on static and gust response solutions SOL 144 and SOL 146, respectively. The wing used for this validation, as shown in Figure 3, is a rectangular strut-braced wing with dimensions and laminate stacking sequences presented in Table 1. Additionally, the wingbox is defined using the composite material properties presented in Table 2 [26]. Last, the flight conditions used for this analysis and the characteristics of the 1-cosine gust applied in the dynamic load case are detailed in Table 3.

As a final remark, it is important to note that this particular geometry was chosen to facilitate easy replication in NX Nastran, thereby enabling a direct comparison of PROTEUS results with the well-established Doublet Lattice Method (DLM) available in NX Nastran.

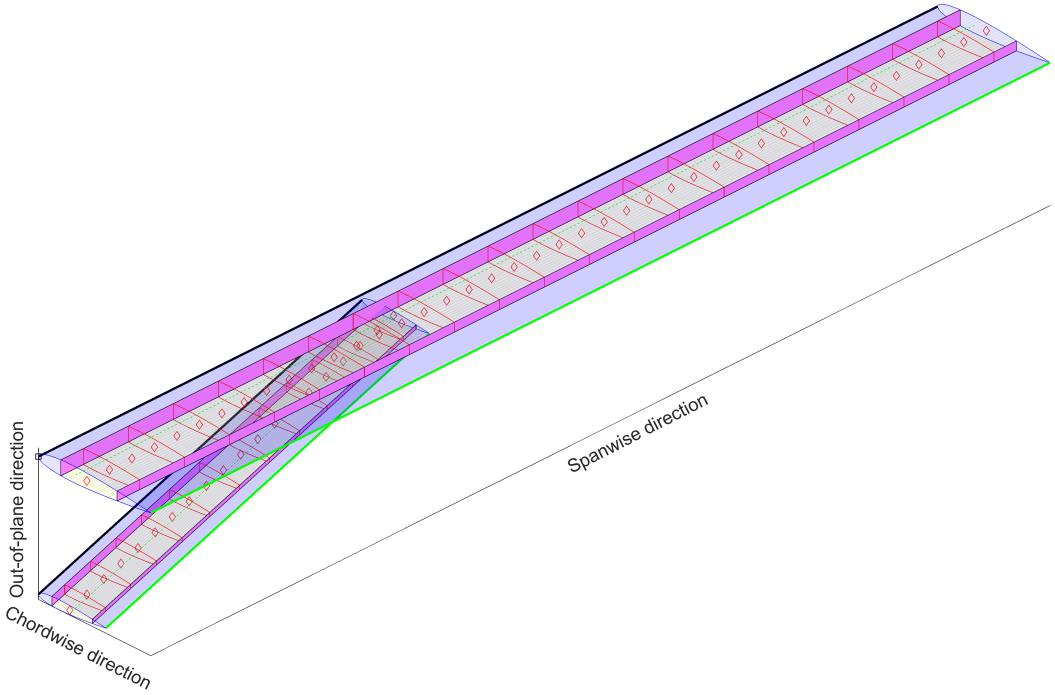

Fig. 3 Representation of the SBW geometry used for study case 1.

Table 1 Main dimensions of the wing model used in study case 1.

Parameters	Main Wing	Strut
Chord, m	2.5	1.5
Root out-of-plane position, m	0	-2.5
Leading edge chordwise position, m	0	0
Tip spanwise position, m	20	7.2
Front spar, % Chord	0.2	0.2
Rear spar, % Chord	0.7	0.8
Rib spacing, m	0.5	0.4
Airfoil	NACA 0012	NACA 0012
Laminate Stacking Sequence	$[-45°_{16}, 45°_{16}, 0°_{16}, 90°_{16}]_s$	

Table 2 Single ply material properties used in study case 1 [26].

E_{11}, GPa	E_{22}, GPa	G_{12}, GPa	ν_{12}, -	Density, kg/m^3	Ply thickness, mm
141	10	7	0.3	1580	0.15

Table 3 Flight conditions of aeroelastic analysis conducted in study case 1.

Load case	EAS, m/s	Mach, -	Angle of attack, deg	Gust frequency, Hz	Gust amplitude, m/s
Static	100	0.4	6	-	-
Dynamic	100	0.4	0	8	10

B. Case 2: Aeroelastic tailoring on a regional aircraft wing

The second study case investigates the impact of aeroelastic tailoring on the structural weight of the high aspect ratio wing designed within the HERWINGT project. The geometry and structural layout for this case, illustrated in Figure 4, along with the materials employed, are supplied by project partners.

In order to assess the effect of aeroelastic tailoring, the wing is discretised in the laminate regions presented in Figure 5 and three separate optimisations are conducted, each employing different laminate options:

1) *Symmetric unbalanced laminates:* the design variables of the optimisation are the eight lamination parameters related to the in-plane and the out-of-plane properties and the thickness of the laminate. In total, each laminate is defined by nine design variables.
2) *Symmetric balanced laminates:* in this case, four of the laminate parameters become zero, resulting in a reduced number of design variables of five per laminate.
3) *Thickness optimisation with a prescribed stacking sequence:* the lamination parameters are predefined according to a symmetric balanced stacking that accounts for the 10% rule while reinforcing the longitudinal direction of the laminate ($[0_{60\%}/\pm45_{30\%}/90_{10\%}]_s$). Consequently, the design variables are reduced to just one per laminate, the thickness.

Previous studies on cantilever wings [27] have observed that constraints applied to the laminate can significantly affect the final weight. Thus, the results of these three optimisations will be compared to assess the impact of laminate constraints on the weight of an SBW design.

To conclude, the load cases (LC) used in this study are detailed in Table 4, where v_c is the design cruise true airspeed (TAS), M_c denotes the cruise Mach number, h_c is the cruise altitude, all of which are project-provided inputs. An asterisk (*) denotes properties that require a correction to account for altitude. Additionally, Table 5 provides a summary of the constraints applied during the optimisation.

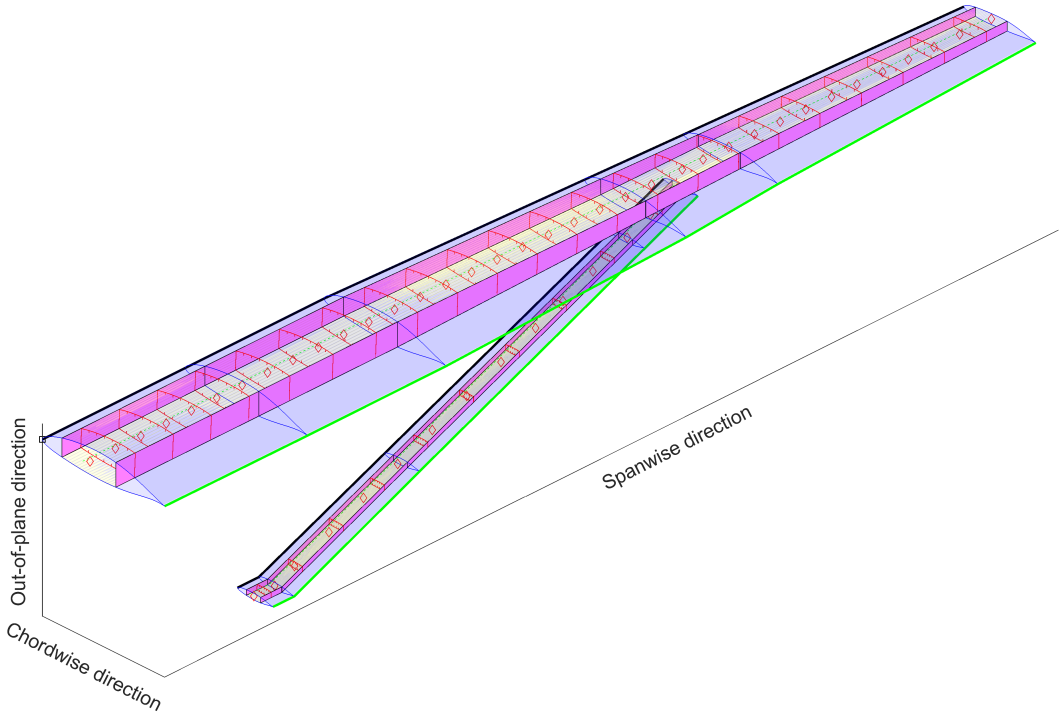

Fig. 4 Representation of the SBW geometry used for the aeroelastic optimisation in study case 2.

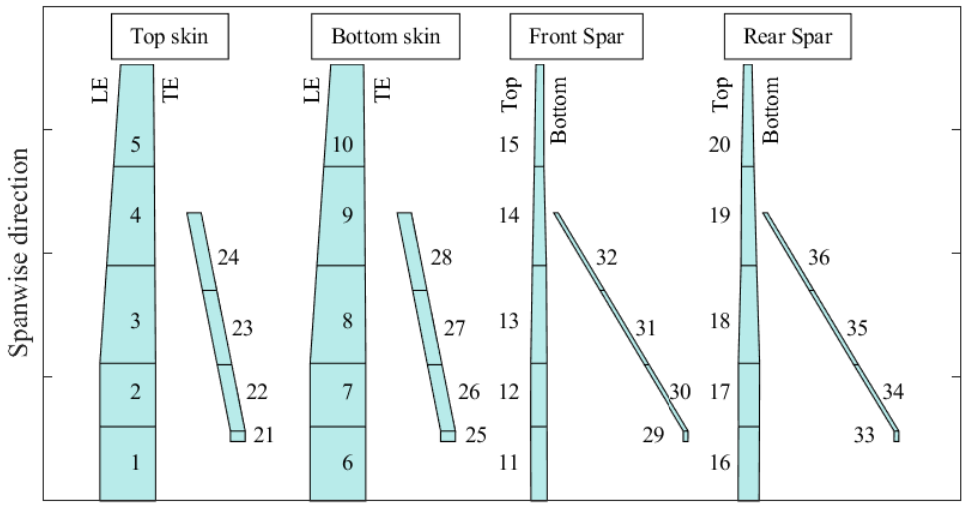

Fig. 5 Laminate discretisation used for the laminate optimisation in study case 2.

Table 4 Summary of load cases used in the optimisation procedure in study case 2.

#LC	TAS, m/s	Mach	EAS, m/s	Altitude, m	Load factor, n	Description
1	v_c	M_c	v_c*	h_c	1	Cruise conditions
2	v_c	M_c*	v_c	0	1	Cruise at sea level
3	v_c	M_c	v_c*	h_c	2.5	Pull-up maneuvre
4	v_c	M_c*	v_c	0	2.5	Pull-up manoeuvre at sea level
5	v_c	M_c	v_c*	h_c	-1	Pull-down manoeuvre
6	v_c	M_c*	v_c	0	-1	Pull-down manoeuvre at sea level

Table 5 Summary of constraints applied to the optimisation in study case 2.

Type	**Description**	**Amount**
Laminate Feasibility	Constrain lamination parameters for feasibility [28]	5 per laminate
Strain	Based on Tsai-Wu failure index [29]	8 per element,laminate and LC
Buckling	Simply supported panel between ribs and stringers	8 per panel and LC
Aeroelastic stability	Linear dynamic analysis around deflected shape	10 eigenvalues per LC
Aileron effectiveness	Definition based on CS-25 AMC 25.147(f) [30]	1 per LC

IV. Results

This section presents the results of the two study cases. Section IV.A focuses on the validation study, while Section IV.B presents the aeroelastic tailoring study.

A. Case 1: Validation

The validation study aims to compare the results obtained with PROTEUS to those obtained in NX Nastran. Starting with the static aeroelastic solution comparison, Figure 6 shows the out-of-plane deflection of the wing, which exhibits very good agreement between both models, with a difference of 6% in the tip displacement between PROTEUS and NX Nastran results. In addition, the Von Mises equivalent strains on the wingbox, presented in Figure 7 to Figure 9, serve to assess the results of the cross-sectional modeller. While the strain distributions generally show good agreement between models, minor differences are observed at the wing-strut junction, which may be attributed to variances in model creation between the different programs, particularly in modelling the attachment.

Next, focusing on the comparison of dynamic results between the linearised dynamic solution from PROTEUS and SOL 146 from NX Nastran, Figure 10 illustrates the wing root reaction forces and moments response to the gust specified in Table 3. PROTEUS captures the main features of the gust response, showing differences below 3% in the spanwise and out-of-plane shear peak loads (Y and Z directions in Figure 2 respectively) and below 10% in the bending and torsional moments peak loads (M_x and M_y respectively). However, PROTEUS and NX Nastran present important differences in the chordwise shear force (X direction in Figure 2) and the lead-lag moment (M_z) responses.

One possible reason for these discrepancies is the combination of the coupling present in the natural modes and the NX Nastran model not including aerodynamic damping in the chordwise direction. First, due to the presence of the strut, the natural modes of the structure show some coupling between the in-plane and out-of-plane deflections. For this reason, an out-of-plane excitation (i.e. the gust) also produces a perturbation in the in-plane direction, as observed in F_x and M_z, the magnitude of which will depend on the damping. On the one hand, PROTEUS includes chordwise aerodynamic damping and, as a result, F_x shows a perturbation one order of magnitude lower than F_y and F_z. On the other hand, the DLM aerodynamic model in NX Nastran does not include damping in the chordwise direction, which leads to higher F_x and M_z peak loads with respect to PROTEUS. Further investigations are planned to verify that this is the reason behind these differences.

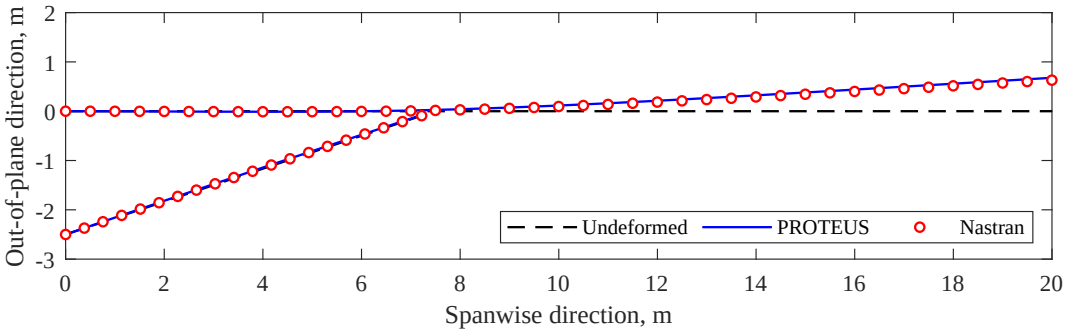

Fig. 6 Comparison of out-of-plane deflections in PROTEUS and NX Nastran.

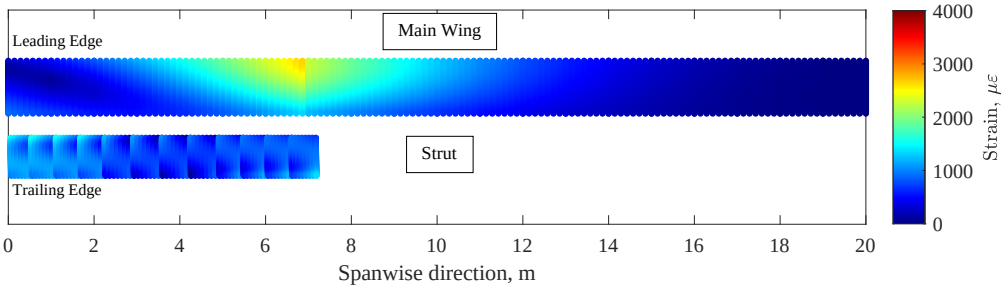

(a) PROTEUS

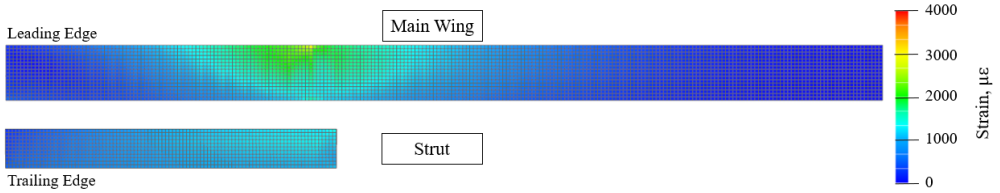

(b) NX Nastran

Fig. 7 Von Mises strain distribution on the wing and the strut top skins. Comparison between PROTEUS and NX Nastran.

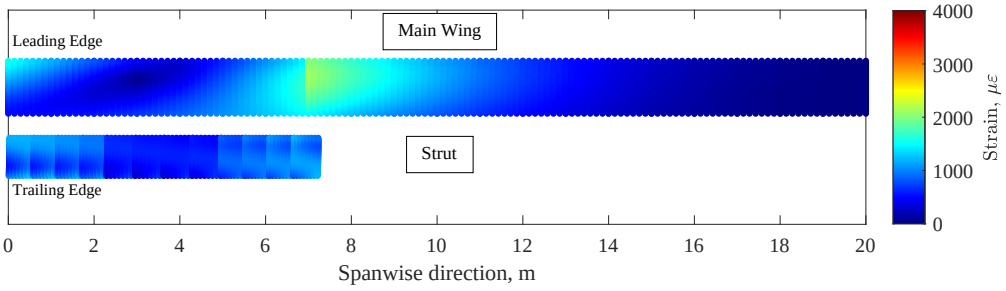

(a) PROTEUS

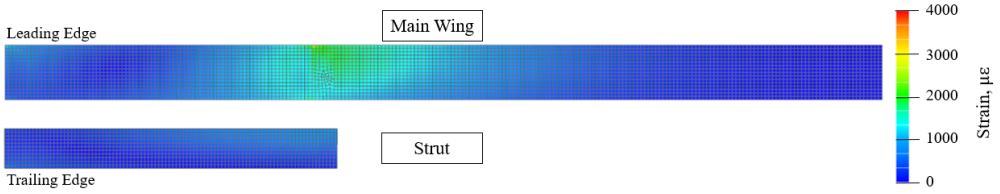

(b) NX Nastran

Fig. 8 Von Mises strain distribution on the wing and the strut bottom skins. Comparison between PROTEUS and NX Nastran.

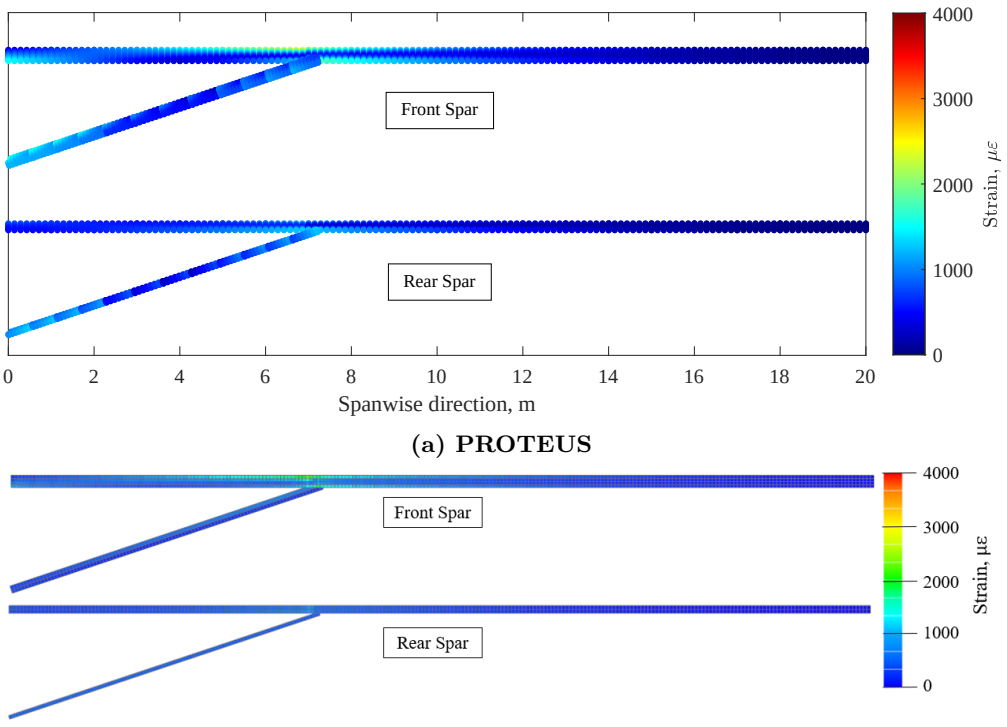

(a) PROTEUS

(b) NX Nastran

Fig. 9 Von Mises strain distribution on the wing and the strut spars. Comparison between PROTEUS and NX Nastran.

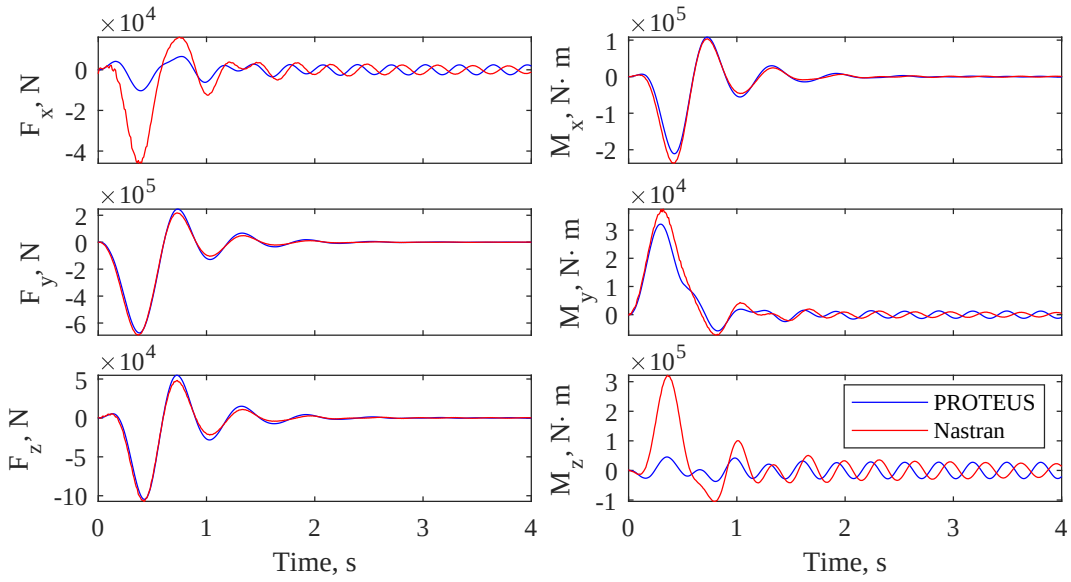

Fig. 10 Comparison of the wing root reaction forces and moments in dynamic load case in PROTEUS and NX Nastran.

B. Case 2: Aeroelastic tailoring on a regional aircraft wing

This part of the study addresses the impact that aeroelastic tailoring can have on the total structural mass by considering different laminate constraints. Table 6 presents a comparison of the wingbox structural mass after optimising the laminates according to the three sets of constraints outlined in Section III.B, providing the structural mass and the mass reduction with respect to the thickness optimisation. In addition, Figure 11 through Figure 13 present the corresponding thickness and laminate stiffness distributions, a concept introduced by Dillinger et al. [31]. These stiffness distributions represent the laminate in-plane and bending stiffnesses as a function of the angle with respect to the laminate longitudinal direction, θ. This is achieved by using the thickness-normalized engineering modulus of elasticity, $\hat{E}_{11}$, and the thickness-normalized bending modulus of elasticity, $\hat{D}_{11}$, respectively.

Table 6 Comparison of wingbox mass for the different optimisation procedures and relative mass reduction with respect to the thickness optimisation.

Component	Thickness	Balanced	Unbalanced
Wing, kg	1572	1002 (-36%)	984 (-37%)
Strut, kg	284	264 (-7%)	260 (-8%)
Total, kg	1856	1266 (-32%)	1244 (-33%)

The results highlight that the thickness optimisation alone places limitations on the weight reduction potential of composite materials. Since the stacking sequence is fixed, only the thickness can be modified, thus the laminates exhibit identical stiffness properties, as can be observed in Figure 11a. However, when balanced and unbalanced laminates are allowed, the material can be tailored to reinforce the main loading directions, resulting in designs more than 30% lighter. This adaptation to local loads can be observed in the stiffness distributions shown in Figure 12a and Figure 13a, where each of the laminates presents different stiffness rosettes. Finally, notice that the thickness optimisation is highly dependent on the selected stacking sequence, since it restricts the capability of tailoring the stiffness to meet the strength and buckling constraints. Therefore, the results might improve if a different stacking sequence was used.

When comparing the unbalanced and balanced designs, there is only a 2% difference in mass, which can be understood when examining the stiffness distribution along the span of the wing and the strut. As can be observed in Figure 12 and Figure 13, the difference between the symmetric balanced and symmetric unbalanced designs is very small. The only noticeable variations occur in the laminates near the wing root (specifically, Laminates 6, 7, and 16), which lead to very similar overall structural mass of the two designs, which is different to the behaviour observed in cantilever wings. Krüger et al. [27] show that, when unbalanced laminates are allowed, the optimisation leads to a design in which the laminates are tailored to provide load alleviation. However, it is not the case in the SBW design optimisation due to the presence of the strut, which alters the deflected shapes of the wing and consequently limits the load alleviation capability. The tip deflections and load distribution are used to illustrate this effect.

First, Table 7 presents the maximum relative out-of-plane tip deflections (n = 2.5) with respect to the wing semi-span for each optimised design. The tip exhibits minimal displacements with a maximum of 1.6% of the semi-span, which is considerably lower than the 8% tip displacement observed for the reference aircraft in similar conditions [32]. This difference in tip displacement with respect to the reference aircraft can be attributed to the modifications in boundary conditions and deflected shapes due to the presence of the strut: the wing is not only constrained at the root but also the wing-strut junction, which strongly limits the out-of-plane and torsional deflections.

Table 7 Relative tip out-of-plane displacement with respect to semi-span for the different optimisation cases.

Optimisation case	Thickness	Balanced	Unbalanced
Tip out-of-plane displacement, % of semi-span	1.4	1.6	1.6

Furthermore, the reduced deflections also affect the capabilities of the laminates to provide aeroelastic tailoring for passive load alleviation. This capability depends on the bend-twist coupling ability of the wing such that a bending deflection can induce a local change in the angle of attack, which becomes apparent when examining the aerodynamic load distribution on the wing. In cantilevered designs allowing unbalanced laminates [27], the lift at the tip is reduced compared to a balanced design to alleviate the root bending moment. At the same time, the lift at the root increases to compensate for the change in the outboard lift. However, in the SBW design, as shown in Figure 14, the load distribution remains nearly unaffected by the change in the laminate design, indicating limited passive load alleviation capabilities of the symmetric-unbalanced laminates.

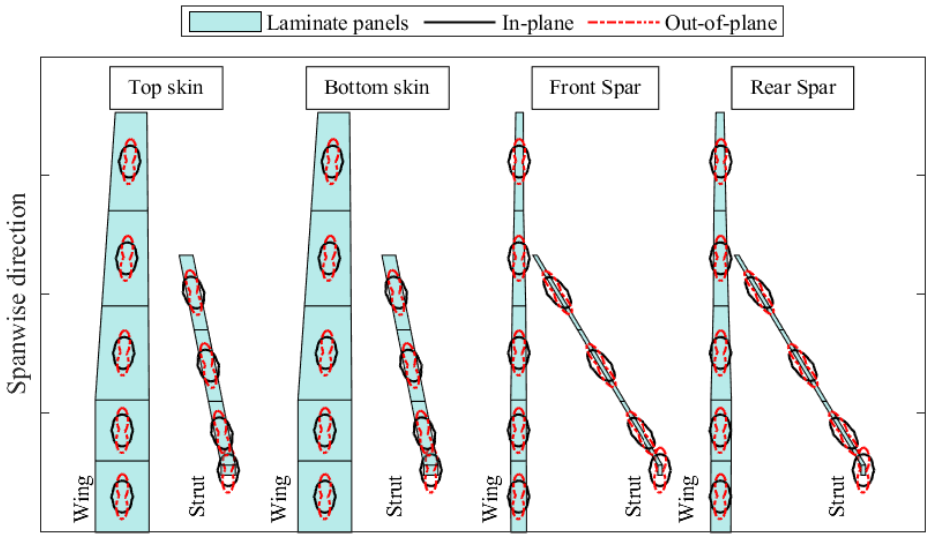

(a) Stiffnes distribution

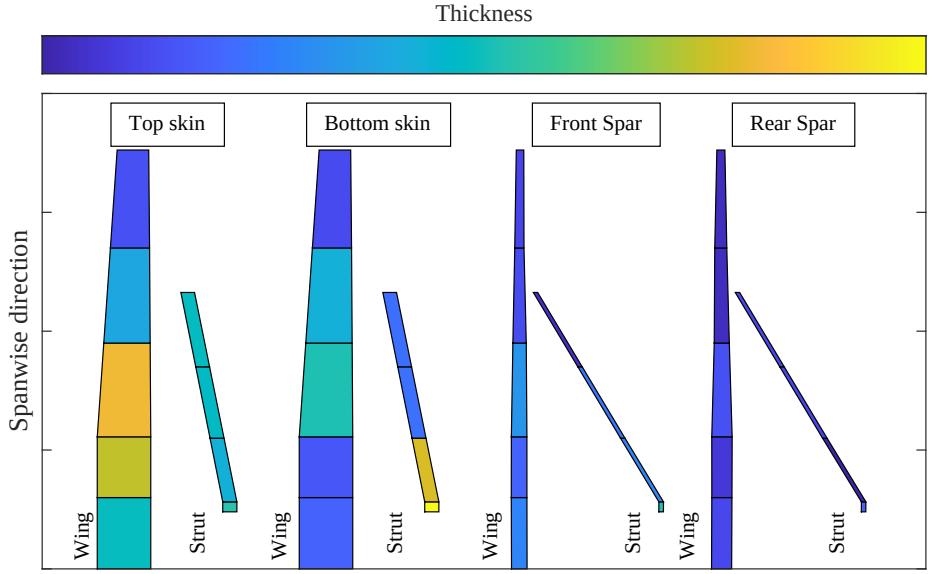

(b) Thickness distribution

Fig. 11 Resulting laminate distribution of the thickness optimisation.

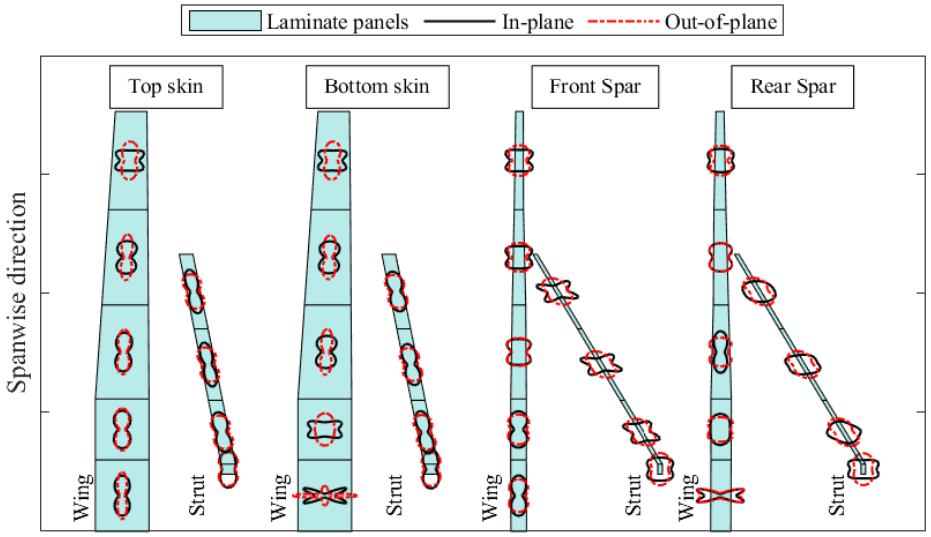

(a) Stiffnes distribution

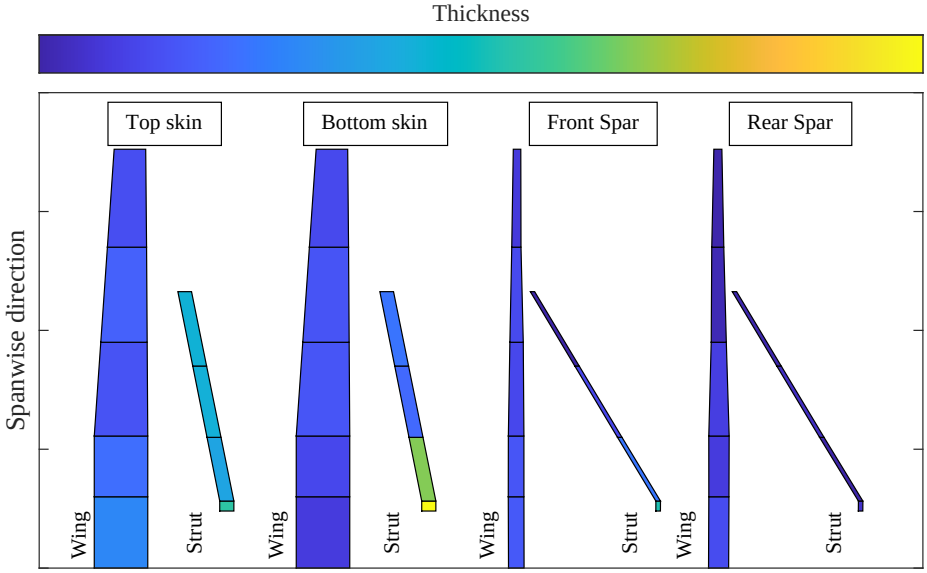

(b) Thickness distribution

Fig. 12 Resulting laminate distribution of the balanced laminate optimisation.

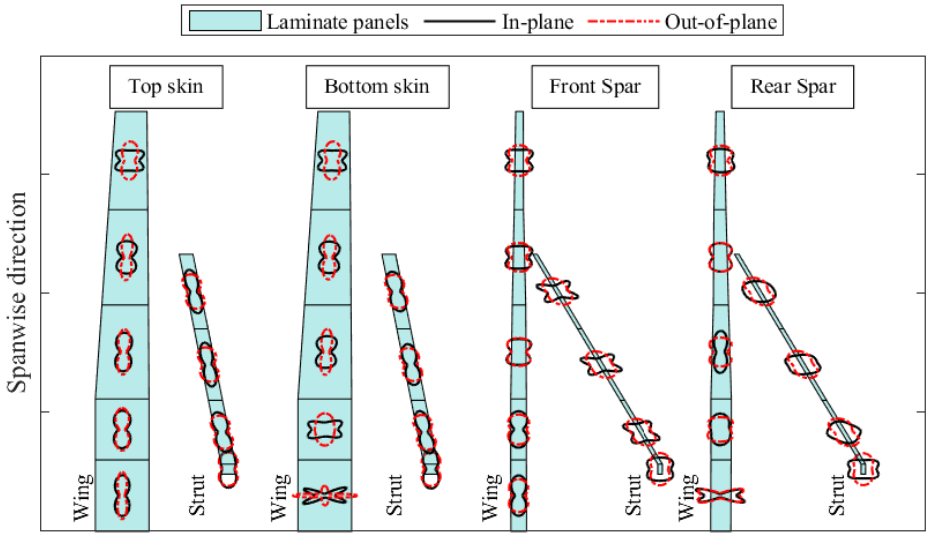

(a) Stiffnes distribution

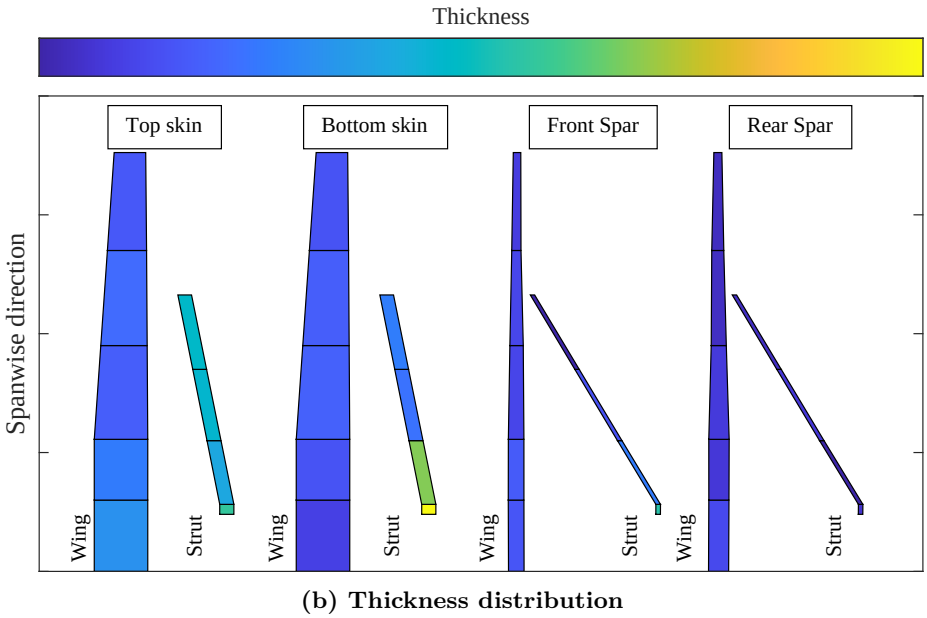

(b) Thickness distribution

Fig. 13 Resulting laminate distribution of the unbalanced laminate optimisation.

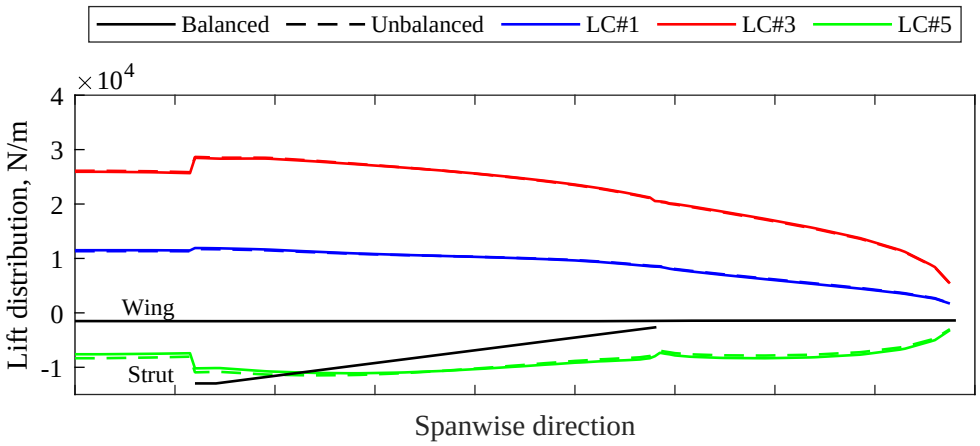

Fig. 14 Lift distribution on the SBW for balanced and unbalanced laminates in different load cases.

V. Conclusions

The presented study has focused on exploring the application of aeroelastic tailoring in the design of a regional aircraft featuring a strut-braced wing. To achieve this goal, the in-house aeroelastic optimisation framework from Delft University of Technology, PROTEUS, has been adapted to account for the strut in the aeroelastic model including all the relevant constraints for the subsequent aeroelastic optimisation. The study consists of two different cases using PROTEUS.

In the first case, a simplified SBW geometry has been used to validate the modifications made to PROTEUS. Both static and dynamic load cases have been compared to a NX Nastran aeroelastic model showing good agreement in terms of displacements, strains and gust response.

The second case involved an assessment of the weight-saving potential associated with aeroelastic tailoring when applied to the high aspect ratio SBW design featured in the HERWINGT project. Considering static load cases and linearised flutter analysis, three optimisation scenarios have been examined: (i) unbalanced symmetric laminates, (ii) balanced symmetric laminates and (iii) thickness optimisation using a prescribed laminate stacking sequence.

Two main conclusions can be drawn from this study. First, the prescribed stacking sequence restricts the ability to tailor the stiffness to effectively meet the strength and buckling constraints, which limits the weight reduction that can be achieved with composites. Considerable weight reduction can be achieved when the optimiser is allowed to tailor the stiffness. However, further research is needed to assess the impact of dynamic load cases.

Second, the current results for the given configuration suggest that the strut has a significant effect on the tailoring capabilities, differing from the trends observed on conventional cantilever wings: tailoring is not as effective due to the strut limiting the wing deflections.

In conclusion, this work has mainly focused on setting up the SBW model and studying the impact of aeroelastic tailoring on the structural mass of the SBW design. However, further analysis is planned to gain a deeper understanding of how the strut modifies loads and deflections compared to a cantilever wing. Additionally, the results presented in this study will be compared to a similar cantilever wing representative of a regional aircraft to quantify the potential benefits of the SBW design. Lastly, the model will be employed for the sizing of an experimental model of a multifunctional strut as part of the HERWINGT project.

Acknowledgements

This study is part of the Hybrid Electric Regional Wing Integration Novel Green Technologies project (HERWINGT). This project has received funding from the Clean Aviation Joint Undertaking under the European Union's Horizon Europe research and innovation programme under grant agreement ID 101102010 (`https://doi.org/10.3030/101102010`).

Views and opinions expressed are however those of the author(s) only and do not necessarily reflect those of the European Union or the Clean Aviation Joint Undertaking. Neither the European Union nor the granting authority can be held responsible for them.

References

[1] "What is ACARE?" ACARE, 2023. URL `https://www.acare4europe.org/about-us/`, [retrieved 24 April 2023].

[2] "Clean Aviation - History," Clean Aviation, 2023. URL `https://www.clean-aviation.eu/about-us/history`, [retrieved 24 April 2023].

[3] European Commission, Directorate-General for Mobility and Transport and Directorate-General for Research and Innovation, *Flightpath 2050 - Europes vision for aviation: maintaining global leadership and serving societys needs*, Publications Office, 2012. https://doi.org/10.2777/15458.

[4] Anderson, J. D., *Fundamentals of aerodynamics*, 6^{th} ed., McGraw Hill, New York, 2017, pp. 450–466.

[5] Gern, F. H., Naghshineh-Pour, A. H., Sulaeman, E., Kapania, R. K., and Haftka, R. T., "Structural Wing Sizing for Multidisciplinary Design Optimization of a Strut-Braced Wing," *Journal of Aircraft*, Vol. 38, No. 1, 2001, pp. 154–163. https://doi.org/10.2514/2.2747.

[6] Gur, O., Bhatia, M., Schetz, J. A., Mason, W. H., Kapania, R. K., and Mavris, D. N., "Design Optimization of a Truss-Braced-Wing Transonic Transport Aircraft," *Journal of Aircraft*, Vol. 47, No. 6, 2010, pp. 1907–1917. https://doi.org/10.2514/1.47546.

[7] Bhatia, M., Kapania, R. K., and Haftka, R. T., "Structural and Aeroelastic Characteristics of Truss-Braced Wings: A Parametric Study," *Journal of Aircraft*, Vol. 49, No. 1, 2012, pp. 302–310. https://doi.org/10.2514/1.C031556.

[8] Chakraborty, I., Nam, T., Gross, J. R., Mavris, D. N., Schetz, J. A., and Kapania, R. K., "Comparative Assessment of Strut-Braced and Truss-Braced Wing Configurations Using Multidisciplinary Design Optimization," *Journal of Aircraft*, Vol. 52, No. 6, 2015, pp. 2009–2020. https://doi.org/10.2514/1.C033120.

[9] Gupta, R., Schetz, J. A., and Kapania, R. K., "Conceptual Design of Complex Transonic Aircraft Configurations with Flutter Prediction," *58th AIAA/ASCE/AHS/ASC Structures, Structural Dynamics, and Materials Conference*, 2017. https://doi.org/10.2514/6.2017-0571.

[10] Droney, C. K., Sclafani, A. J., Harrisson, N. A., Grasch, A. D., and Beyar, M. D., "Subsonic Ultra-Green Aircraft Research Phase III: Mach 0.745 Transonic Truss-Braced Wing Design," Tech. rep., NASA, 2020. CR-2020-5005698.

[11] Harrison, N. A., Gatlin, G. M., Viken, S. A., Beyar, M., Dickey, E. D., Hoffman, K., and Reichenbach, E. Y., "Development of an Efficient M=0.80 Transonic Truss-Braced Wing Aircraft," *AIAA Scitech 2020 Forum*, 2020. https://doi.org/10.2514/6.2020-0011.

[12] Carrier, G. G., Atinault, O., Dequand, S., Hantrais-Gervois, J., C.Liauzun, Paluch, B., Rodde, A., and Toussaint, C., "Investigation of a strut-braced wing configuration for future commercial aircraft," *28th Congress of the International Council of Aeronautical Sciences, ICAS 2012*, 2012.

[13] Moerland, E., Pfeiffer, T., Böhnke, D., Jepsen, J., Freund, S., Liersch, C. M., Chiozzotto, G. P., Klein, C., Scherer, J., Hasan, Y. J., and Flink, J., "On the Design of a Strut-Braced Wing Configuration in a Collaborative Design Environment," *17th AIAA Aviation Technology, Integration, and Operations Conference*, 2017. https://doi.org/10.2514/6.2017-4397.

[14] Carrier, G. G., Arnoult, G., Fabbiane, N., Schotte, J.-S., David, C., Defoort, S., Benard, E., and Delavenne, M., "Multidisciplinary analysis and design of strut-braced wing concept for medium range aircraft," *AIAA SCITECH 2022 Forum*, 2022. https://doi.org/10.2514/6.2022-0726.

[15] Ma, Y., Karpuk, S., and Elham, A., "Conceptual design and comparative study of strut-braced wing and twin-fuselage aircraft configurations with ultra-high aspect ratio wings," *AIAA AVIATION 2021 FORUM*, 2021. https://doi.org/10.2514/6.2021-2425.

[16] Torrigiani, F., Bussemaker, J., Ciampa, P. D., Fioriti, M., Tomasella, F., Aigner, B., Rajpal, D., Timmermans, H., Savelyev, A., and Charbonnier, D., "Design of the Strut Braced Wing aircraft in the AGILE Collaborative MDO Framework," *31st Congress of the International Council of Aeronautical Sciences, ICAS 2018*, 2018.

[17] Rajpal, D., De Breuker, R., Timmermans, H., Lammen, W., and Torrigiani, F., "Including Aeroelastic Tailoring in the conceptual design process of a composite strut braced wing," *31st Congress of the International Council of Aeronautical Sciences, ICAS 2018*, 2018.

[18] Rajpal, D., and De Breuker, R., "Dynamic aeroelastic tailoring of a strut braced wing including fatigue loads," *International Forum on Aeroelasticity and Structural Dynamics, IFASD 2019*, 2019.

[19] "Hybrid Electric Regional Wing Integration Novel Green Technologies - HERWINGT," Cordis, 2023. URL https://cordis.europa.eu/project/id/101102010, [retrieved 29 September 2023].

[20] "Hybrid Electric Regional Wing Integration Novel Green Technologies - HERWINGT Project," EASN-TIS, 2023. URL https://herwingt-project.eu/home, [retrieved 29 September 2023].

[21] Werter, N., and De Breuker, R., "A novel dynamic aeroelastic framework for aeroelastic tailoring and structural optimisation," *Composite Structures*, Vol. 158, 2016, pp. 369–386. https://doi.org/10.1016/j.compstruct.2016.09.044.

[22] Tsai, S., and Pagano, N., "Invariant Properties of Composite Materials," *Composite Materials Workshop*, Westport: Technomic Publishing Co., 1968, pp. 233–253.

[23] Ferede, E., and Abdalla, M., "Cross-sectional modelling of thin-walled composite beams," *55th AIAA/ASME/ASCE/AHS/ASC Structures, Structural Dynamics, and Materials Conference*, 2014. https://doi.org/10.2514/6.2014-0163.

[24] Katz, J., and Plotkin, A., *Low-Speed Aerodynamics*, 2nd ed., Cambridge University Press, 2001.

[25] Svanberg, K., "A Class of Globally Convergent Optimization Methods Based on Conservative Convex Separable Approximations," *SIAM Journal on Optimization*, Vol. 12, No. 2, 2002, pp. 555–573. https://doi.org/10.1137/S1052623499362822.

[26] "HexPly 8552 - Product Data Sheet," Hexcel, 2023. URL https://www.hexcel.com/user_area/content_media/raw/HexPly_8552_eu_DataSheet(1).pdf, [retrieved 2 November 2023].

[27] Krüger, W. R., Meddaikar, Y. M., Dillinger, J. K. S., Sodja, J., and De Breuker, R., "Application of Aeroelastic Tailoring for Load Alleviation on a Flying Demonstrator Wing," *Aerospace*, Vol. 9, No. 10, 2022. https://doi.org/10.3390/aerospace9100535.

[28] Raju, G., Wu, Z., and Weaver, P., *On Further Developments of Feasible Region of Lamination Parameters for Symmetric Composite Laminates*, 2014. https://doi.org/10.2514/6.2014-1374.

[29] IJsselmuiden, S. T., Abdalla, M. M., and Gürdal, Z., "Implementation of Strength-Based Failure Criteria in the Lamination Parameter Design Space," *AIAA Journal*, Vol. 46, No. 7, 2008, pp. 1826–1834. https://doi.org/10.2514/1.35565.

[30] "CS-25 Amendment 27," EASA, 2023. URL https://www.easa.europa.eu/en/document-library/certification-specifications/cs-25-amendment-27, [retrieved 30 October 2023].

[31] Dillinger, J. K. S., Klimmek, T., Abdalla, M. M., and Gürdal, Z., "Stiffness Optimization of Composite Wings with Aeroelastic Constraints," *Journal of Aircraft*, Vol. 50, No. 4, 2013, pp. 1159–1168. https://doi.org/10.2514/1.C032084.

[32] Kidane, B. S., and Troiani, E., "Static Aeroelastic Beam Model Development for Folding Winglet Design," *Aerospace*, Vol. 7, No. 8, 2020. https://doi.org/10.3390/aerospace7080106.